816–825 *Nucleic Acids Research, 2006, Vol. 34, No. 3*
doi:10.1093/nar/gkj481

Structure of the *Tetrahymena thermophila* telomerase RNA helix II template boundary element

Rebecca J. Richards[1], Carla A. Theimer[1], L. David Finger[1] and Juli Feigon[1,2,*]

[1]Department of Chemistry and Biochemistry and [2]Molecular Biology Institute, University of California, Los Angeles, CA 90095-1569, USA

Received December 12, 2005; Revised and Accepted January 14, 2006

ABSTRACT

Telomere addition by telomerase requires an internal templating sequence located in the RNA subunit of telomerase. The correct boundary definition of this template sequence is essential for the proper addition of the nucleotide repeats. Incorporation of incorrect telomeric repeats onto the ends of chromosomes has been shown to induce chromosomal instability in ciliate, yeast and human cells. A 5′ template boundary defining element (TBE) has been identified in human, yeast and ciliate telomerase RNAs. Here, we report the solution structure of the TBE element (helix II) from *Tetrahymena thermophila* telomerase RNA. Our results indicate that helix II and its capping pentaloop form a well-defined structure including unpaired, stacked adenine nucleotides in the stem and an unusual *syn* adenine nucleotide in the loop. A comparison of the *T.thermophila* helix II pentaloop with a pentaloop of the same sequence found in the 23S rRNA of the *Haloarcula marismortui* ribosome suggests possible RNA and/or protein interactions for the helix II loop within the *Tetrahymena* telomerase holoenzyme.

INTRODUCTION

Telomerase is the ribonucleoprotein (RNP) complex responsible for maintenance of the telomeric DNA at the physical ends of chromosomes. Telomeres are composed of a repeating sequence of nucleotides, TTGGGG in ciliates and TTAGGG in vertebrates, as well as a number of accessory telomere binding proteins (1). Telomere shortening occurs during successive rounds of chromosomal replication and can lead to end-to-end fusions, degradation and the eventual loss of genetic information (2). The incorporation of incorrect telomeric repeats onto the ends of chromosomes has been found to induce chromosomal instability and to compromise cellular viability in ciliate, yeast and human cells (3–5). Telomerase was first discovered and has been extensively studied in the ciliate *Tetrahymena thermophila* (6,7). Ciliates possess two morphologically and functionally different nuclei, a micronucleus and a macronucleus. While the micronucleus is transcriptionally silent and specialized for sexual exchange, the macronucleus is extremely transcriptionally active, containing ~20 000 chromosomes and 40 000 telomeres. This exceptional abundance of telomeres results in ciliates having very high levels of telomerase activity compared with other organisms.

The *T.thermophila* telomerase RNP holoenzyme has been characterized by affinity purification and consists of a catalytic protein component, TERT (telomerase reverse transcriptase), an intrinsic RNA component, TER (telomerase RNA), which includes the telomeric template sequence, and four other associated proteins, p20, p45, p65 and p75 (8). Although the primary sequence of the catalytic domain and general functional characteristics of TERT are related to those of retrotransposon and retroviral reverse transcriptases (RTs), the mechanism of reverse transcription differs significantly (9). *In vivo*, retroviral reverse transcriptases copy viral genomic RNA into DNA, while *in vitro*, they reverse transcribe any single-stranded RNA sequence provided a primer is present to initiate synthesis. In both cases, the reverse transcriptase associates with the template in a sequence-independent fashion that promotes mobility and single-nucleotide addition processivity along the entire length of the RNA sequence. Synthesis of the telomere repeat requires both the TERT and TER components, and TERT uses a small portion of the bound TER RNA as an internal template to repetitively copy a short and specific sequence to extend the telomeric substrate. Thus, in addition to single-nucleotide addition processivity, as seen for retroviral reverse transcriptases, telomerase activity requires translocation and repeat-addition processivity to add multiple telomeric repeats to the same DNA substrate before dissociating. Because telomerase must faithfully

*To whom correspondence should be addressed. Tel: +1 310 206 6922; Fax: +1 310 825 0982; Email: feigon@mbi.ucla.edu

copy only a small, yet very specific, portion of TER, a mechanism for the proper definition of the template boundaries is required.

The telomerase RNA component is divergent in primary sequence and in length across species ranging from ~150 nt in ciliates and 400–600 nt in vertebrates to ~1300–1500 nt in yeast. Despite vast differences in sequence and length, all telomerase TERs identified to date contain a short template sequence complementary to the telomeric repeat and a set of similar secondary structural elements (10–12). These elements include, in addition to the telomeric template sequence, a potential hairpin (H)-type RNA pseudoknot, a long-range base paired helix enclosing the template and pseudoknot, and a template boundary-defining element (10–12).

The *T.thermophila* TER is 159 nt long and contains four helices, I-IV, each with its own specific function in telomerase activity, as well as several functionally significant single-stranded regions (Figure 1A). Helix I is involved in long-range base pairing and establishes the overall topology of the RNA. Its sequence as well as structure has recently been identified as critical for high affinity TERT binding (13). Helix II contains part of the element required for 5′ template boundary definition, the template boundary element (TBE). The remaining portion of the TBE is located in the single-stranded regions immediately 5′ and 3′ of helix II and interacts with the RNA binding domain of TERT (13). Between helices II and III is a single-stranded region containing the template sequence, 5′-CAACCCCAA-3′, complementary to the *Tetrahymena* telomeric repeat, as well as nucleotides 3′ of the template required for template recognition (14). Helices IIIa and IIIb have been proposed to form an H-type RNA pseudoknot involved in RNP assembly *in vivo* (15) and repeat-addition processivity (16). Helix IV is involved in nucleotide addition processivity, interacts with the N-terminal region of TERT, and makes possible contacts with the template recognition element (TRE) 3′ of the template (13,16,17). Helix IV also binds the telomerase associated protein p65, which aids in the recruitment of TERT to TER (18).

The template boundary element (TBE) is responsible for defining the 5′ boundary of the template. In *Tetrahymena*, the conserved 5′-(CU)GUCA-3′ sequence (nt 35–40) as well as base pairing interactions at the proximal end of helix II (C19·G37 base pairing) have been implicated in proper template boundary definition (19,20) (Figure 1A). The correct identity of the nucleotides at positions 15 and 16 upstream of helix II are required for TERT binding and thus are also essential for proper template boundary definition (21). In ciliates, yeast and most vertebrates, the TBE is located close to and upstream of the template sequence and is separated from the template by a short uridine-rich stretch of single-stranded nucleotides (22). In addition, almost all TBEs are predicted to adopt some type of helical structure. The only exception is the mouse telomerase RNA, which does not possess a helix upstream of the template. Instead, the mouse 5′ template boundary is defined by the 5′ end of the RNA, located 2 nt upstream of the template. Addition of a 5′ helix to the mouse telomerase RNA increases the processivity of mouse telomerase suggesting that a template boundary helix located 5′ of the template provides an optimal RNA structure for telomerase function (22).

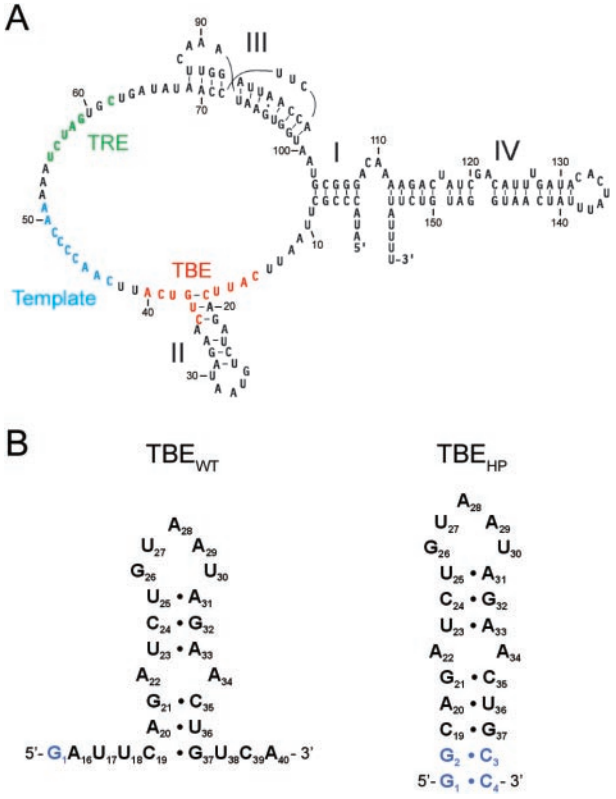

Figure 1. The *T.thermophila* telomerase TBE. (**A**) Secondary structure of the *T.thermophila* telomerase RNA, with helices and specific functional domains identified as previously described (13). The template boundary element (TBE), template recognition element (TRE) and telomere template are indicated in red, green and blue, respectively. (**B**) Secondary structure of the TBE_{WT} and TBE_{HP} constructs. Residues are numbered to match the full length TER. Blue nucleotides indicate non-native sequences added during construct design.

The mechanism of telomere addition is not yet completely defined, although biochemical studies over the last 20 years have greatly improved our understanding of telomerase function. Proper template boundary definition is an important component of telomerase activity. In this study, we have determined the solution structure of the template boundary element from *T.thermophila*. Helix II forms a duplex that is capped by a structured pentaloop containing a *syn* adenine nucleotide. Within the duplex, two adenines on opposing strands are stacked into the helix forming a staggered adenine motif. In the large ribosomal subunit, a pentaloop with the same sequence found in the 23S rRNA interacts with both RNA and protein (23,24) suggesting a possible role for this loop in RNA and/or protein interactions in the telomerase holoenzyme. The 3D structure of helix II from *Tetrahymena* telomerase including the single-stranded flanking 5′ and 3′ regions may help identify how the essential step of template boundary definition is accomplished by the telomerase holoenzyme.

MATERIALS AND METHODS

RNA synthesis and sample preparation

Unlabeled and ^{13}C,^{15}N uniformly-labeled RNA oligonucleotides (Figure 1B) were synthesized using *in vitro* transcription

with T7 RNA polymerase and synthetic DNA oligonucleotides, and purified as described previously (25). Unlabeled nucleoside triphosphates (NTPs) were purchased from Pharmacia, and individual ^{13}C, ^{15}N-labeled NTPs were purchased from Silantes. Purified RNAs were annealed at 95°C in H_2O under dilute conditions and then concentrated and exchanged into NMR buffer by ultrafiltration (10 mM sodium phosphate, pH 6.7, 30 mM KCl, 50 μM EDTA, 0.2% NaN_3) using Amicon filtration devices. NMR sample concentrations were ~1 mM. The salt concentration in NMR samples was kept low to prevent dimer formation. For spectra collected in H_2O (H_2O samples), 5% D_2O was added and for spectra collected in D_2O (D_2O samples) the RNA was lyophilized and redissolved in 99.998% D_2O 2–3 times.

UV melting

Thermal melting experiments were collected on a Beckman DU800 spectrophotometer equipped with a six-cell block and Peltier temperature controller. Absorbance was recorded as a function of temperature at 260 and 280 nm simultaneously. RNA samples (2–4 μM) were prepared by dilution of NMR samples, heated at 65°C for 10 min, slow cooled to room temperature and then equilibrated at 5.0°C for 20 min prior to data collection. The temperature was increased at a rate of 0.4°C/min from 5 to 98°C. Once collected, the melting data were subjected to smoothing (window = 4°C) and the melting profile was obtained by taking the first derivative of the absorbance with respect to the temperature ($\partial A/\partial T$). The melting profile was then analyzed using a non-linear least squares parameter estimation of $T_{m,i}$ (melting temperature), H_i (van't Hoff enthalpy), A_i^{260} (amplitude of $\partial A/\partial T$ at 260 nm) and A_i^{280} (amplitude of $\partial A/\partial T$ at 280 nm) for each *i*th transition upon application of a sequential two-state unfolding model using the *tmelt* program (26).

NMR spectroscopy

NMR spectra were collected on Bruker DRX 500, 600 and 800 MHz spectrometers. Exchangeable proton spectra were measured in H_2O samples at 283K, and nonexchangeable proton spectra were measured in D_2O samples at 293K. Exchangeable protons and nitrogens in the Watson–Crick base pairs were assigned using 2D NOESY, ^1H-^{15}N HMQC and ^{15}N-correlated CPMG-NOESY spectra (27). Hydrogen bonding patterns were confirmed for the Watson–Crick base pairs using J_{NN}-HNN COSY (28). The adenine nitrogen resonances were assigned using long range (H2)-(N1,N3) HSQC (29) and 2D (H)N(C)-TOCSY-(C)H (30) experiments. Non-exchangeable protons and carbons were assigned using 2D NOESY, homonuclear TOCSY, ^1H-^{13}C CT-HSQC, 2D HCCH-COSY, 3D HCCH-TOCSY, 3D HMQC-NOESY and 3D HCN experiments (27). $^3J_{H3'P}$ and $^3J_{CP}$ were measured using ^{31}P spin echo difference CT-HSQCs to determine the β and ε torsion angles (31,32). Phosphorus assignments were analyzed using a combination of ^{31}P 1D and proton detected ^1H-^{31}P heteronuclear correlation (HETCOR) spectra (33). Residual dipolar couplings (RDCs) were measured for $^1J_{HC}$ in 3% C12E6/hexanol using CT-CE-HSQC (34). Spectra were processed and analyzed using Bruker XWINNMR 2.6 and Aurelia 3.108.

Structure calculations

Interproton distances from 2D NOESY and 3D NOESY-HMQC spectra were generated as described previously (35), except for the classification of semi-quantitative NOEs, which were as follows: strong (1.8–3.5 Å), medium (2.5–4.5 Å), weak (3.5–5.5 Å) and very weak (4.5–6.5 Å). In total, 255 intranucleotide and 262 internucleotide non-redundant distance restraints were measured. We used 103 dihedral angle constraints for α, β, γ, δ, ε and ζ backbone angles. The γ dihedral angle for the nucleotides involved in base pairs in the helix were constrained to the A-form value (54 ± 30°). A 1D ^{31}P experiment indicated that two residues had a phosphorus chemical shift outside of the normal range observed for A-form helices. These phosphates were assigned to U27pA28 and U30pA31 using a ^1H-^{31}P heteronuclear correlation experiment to correlate the phosphate chemical shift to the H3′ proton chemical shift (33). Experimentally, the ^{31}P shift shows a linear correlation with changes in ε; therefore, the unusual phosphorus shifts could be attributed to ε angles in the *trans* range (36). Due to the unusual phosphate chemical shifts, the α and ζ torsion angles for these nucleotides were left unconstrained while in all other residues these angles were constrained to the normal *gauche*$^{+/-}$ range of 0 ± 120° during structure calculations. After structure calculation, the α and ζ dihedral angles for U27 and U30 were observed to fall within the normal range seen in A-form stacking regions (36). Nucleotides with observable H1′–H2′ and H1′–H3′ correlations in a 50 ms mixing time TOCSY were constrained as C2′-*endo* (South, 145 ± 30°), nucleotides with observable H1′–H2′ correlations only were constrained to 120 ± 60°, while all other nucleotides which had no detectable H1′–H2′ correlation were constrained as C3′-*endo* (North, 82 ± 30°). Intranucleotide H1′ to aromatic NOEs from a 50 ms 2D NOESY indicated that all nucleotides were *anti* and could thus be constrained to a χ value of −160 ± 30°, except for A29 which was identified as *syn* and was constrained to a χ value of 60 ± 30°. Initial structure calculations included hydrogen bonding distance restraints and weak planarity restraints for the Watson–Crick base pairs only (force constant of 1 kcal/Å^2).

Starting from an extended, unfolded RNA conformation the structures of TBE_{HP} were calculated using XPLOR-NIH 2.9.8 (37,38) using the NOE-derived distances and dihedral angle restraints. The folding and refinement stages followed standard XPLOR protocols. Structures with no experimental restraint violations from the initial 200 calculated structures were then subjected to refinement against 25 residual dipolar couplings. The protocol involved slow cooling from 1000 to 100K in 18 cycles of molecular dynamics corresponding to a total of 18 ps. During this stage, the force constant for dipolar couplings was slowly increased from 0.001 to 0.2 kcal mol^{-1} Hz^{-2}. The experimentally derived RDCs together with the lowest energy structure from the structure calculation employing NOE and dihedral restraints were used as input information. The grid search for the values of the magnitude and asymmetry of the alignment tensor produced optimal values of $D_a = -18$ Hz and $R = 0.65$. The force constants used in the refinement stage of structure calculations were 50 kcal mol^{-1} Å^{-2}, 200 kcal mol^{-1} deg^{-2} and 0.2 kcal mol^{-1} Hz^{-2} for NOEs, dihedral angles and RDCs, respectively. Structural statistics for the 20 lowest energy

Table 1. Structural statistics for TBE_{HP}

Experimental data used for structure calculations	
NOE-derived distance restraints	
Intranucleotide NOEs	255
Internucleotide NOEs	262
Hydrogen bond for paired residues	21
Dihedral restraints	103
Residual dipolar couplings $^1D_{C-H}$ (Hz)	25
Base pair planarity restraints	8
RMS deviation from experimental restraints[a]	
Distance restraints (Å)[b]	0.006 ± 0.004
Dihedral restraints (°)[c]	0.092 ± 0.083
Dipolar couplings (Hz)	0.294 ± 0.078
Deviations from idealized geometry[a]	
Bonds (Å)	0.004 ± 0.0001
Angles (°)	1.030 ± 0.004
Impropers (°)	0.361 ± 0.004
Overall RMS deviation (Å)[a]	
From mean structure	0.78 ± 0.15

[a]Averaged over the accepted structures.
[b]No violations > 0.2 Å.
[c]No violations > 5°.

structures are presented in Table 1. All structures were viewed and analyzed using MOLMOL (39).

Coordinate deposition

The coordinates for the 20 lowest energy structures of TBE_{HP} have been deposited to the Protein Data Bank, accession code 2FRL.

RESULTS

RNA construct design

Two NMR constructs were investigated for structure determination of the *T.thermophila* TER helix II template boundary element, TBE_{WT} and TBE_{HP} (Figure 1B). TBE_{WT} consists of nt 16–40 from the *T.thermophila* telomerase RNA with a single G added to the 5′ end of the sequence for *in vitro* transcription by T7 RNA polymerase. This sequence contains all of helix II as well as the single-stranded regions flanking the helix in both the 5′ and 3′ directions required for template boundary definition (20,21). The imino region of the 2D H_2O NOESY spectrum shows that TBE_{WT} forms all six predicted Watson–Crick base pairs in the helix II stem (Figure 2A). The cross peaks in the 2D D_2O NOESY spectra were well dispersed with NOEs suggesting well-defined structures for both the unpaired adenines in the stem and the capping pentaloop (Figure 2B). The 5′ and 3′ single-stranded regions showed no evidence of base pairing and very few NOEs, consistent with a mostly unstructured region (Figure 2B and data not shown). The melting temperature (T_m) of the TBE_{WT} RNA under the NMR solution conditions is 46.4°C, indicating a low thermodynamic stability. Because the single-stranded regions did not show any evidence of structure, a more stable construct, TBE_{HP}, was designed (Figure 1B). TBE_{HP} has the 5′ and 3′ single-stranded nucleotides removed, leaving the native sequence from 19 to 37, and two Watson–Crick G·C base pairs added at the end of the helical stem for added stability and increased *in vitro* transcription efficiency. TBE_{HP} has imino resonances for all eight of the predicted base pairs in the A-form stem, full sequential base/H1′ connectivities (Figure 2A and B), and a much higher melting temperature (68.5°C) than the original TBE_{WT} construct. Comparison of the 2D NOESY aromatic/H1′ regions of TBE_{WT} and TBE_{HP} shows that they are nearly identical (Figure 2B), and a comparison of H1′, H6/H8 and H5/H2 chemical shifts for the common nucleotides (C19–G37) shows that they are essentially identical except at the end of the helix as expected (Figure 2C). The chemical shift differences >0.1 p.p.m. observed for C19 and G37 at the end of the TBE helix are due to differences in base stacking interactions for TBE_{WT} and TBE_{HP}.

NMR spectroscopy of the TBE

Essentially complete ^1H and protonated-^{13}C and -^{15}N assignments of TBE_{HP} were obtained using a combination of homonuclear and heteronuclear 2D and 3D NMR experiments on unlabeled and uniformly ^{13}C,^{15}N-labeled samples prepared in D_2O and H_2O (see Materials and Methods). Assignment of the base/H1′ region of the 2D D_2O NOESY spectrum shows NOEs consistent with formation of an A-form helix from G1 to U25 and A31 to C4 (Figure 1B). The H_2O and D_2O NOE patterns indicate that A22 and A34 are both stacked into the helix, but there is no evidence of hydrogen bonding interactions between A22 and A34. The N1 chemical shifts for both A22 and A34 are shifted downfield from the N1 resonances for adenines in Watson–Crick base pairs and are much less intense in the long range (H2)-(N1,N3) HSQC (29). The 2D D_2O NOESY (50 ms) contains a strong H2 to H2 NOE indicating that the A22 and A34 H2s are in close proximity. The normal H2/H1′ NOE pattern observed in A-form RNA helices is observed for both the A22 H2 and A34 H2; however, the A22 H2 has a much stronger NOE to the U23 H1′ than the C35 H1′, while the A34 H2 has a much stronger NOE to the C35 H1′ than to the U23 H1′ (Figure 2B).

In the pentaloop, a weak imino resonance was identified for G26, but no hydrogen bonding interactions were detected for any of the loop residues. An exchangeable NOE between the imino proton of G26 and the amino proton of A31, as well as nonexchangeable NOEs observed from G26 to U25, indicate conservation of near A-form geometry. Consistent with a well-structured small loop, many NOEs are observed between the loop nucleotides U27, A28, A29 and U30. The very strong A29 H8 to H1′ intraresidue NOE and the downfield shifted A29 H2′ and H3′ resonances (4.88 and 5.05 p.p.m., respectively) indicate that this loop nucleotide is in a *syn* conformation (Figure 2B).

Solution structure of the *T.thermophila* TBE

The NMR structural data indicate that the template boundary element of *T.thermophila* telomerase RNA forms a well-defined 3D structure. The structure determination of TBE_{HP} included 517 NOE distance restraints for an average of 22.5 NOE restraints per nucleotide, 103 dihedral angle restraints and 25 residual dipolar couplings (Table 1). Superposition of the 20 lowest energy structures was performed over all heavy atoms yielding an RMSD to the mean of 0.78 ± 0.15 Å for the ensemble (Figure 3A).

The TBE_{HP} structure shows that residues 19–25 and 31–37 form a continuous A-form helical stem containing all eight of

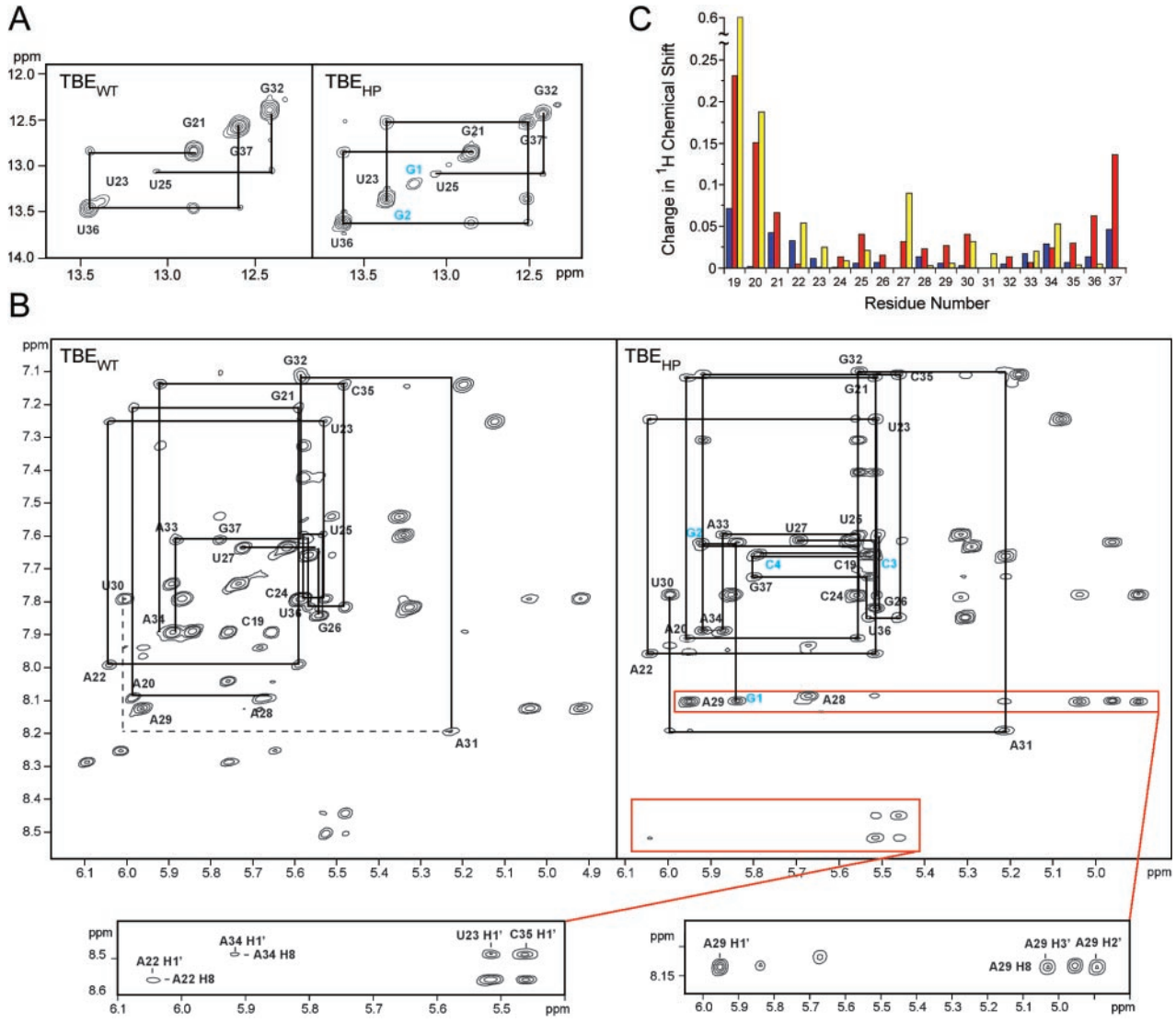

Figure 2. Comparative NMR spectra for TBE_{WT} and TBE_{HP} constructs. (**A**) Imino–imino region of the 2D H_2O NOESY (τ = 100 ms) for TBE_{WT} (left) and TBE_{HP} (right). (**B**) Aromatic-H1′ region of the 2D D_2O NOESY (τ = 300 ms) of TBE_{WT} (left) and TBE_{HP} (right). Horizontal and vertical lines indicate the aromatic to H1′ sequential connectivities, and nucleotide assignments are indicated. The labels for nucleotides added to stabilize the helix in TBE_{HP} are in blue. The regions highlighted with red boxes and expanded below show the A22 and A34 H2 NOEs consistent with A-form stacking and the A29 NOEs indicating a *syn* conformation. (**C**) Histogram of the chemical shift differences between TBE_{WT} and TBE_{HP}. Bars indicate H1′ (blue), H6/H8 (red) and H5/H2 (yellow) chemical shift differences between the nucleotides in common, respectively.

the predicted Watson–Crick base pairs (Figure 3B). The two unpaired adenine nucleotides, A22 and A34, show no dihedral angle deviations from A-form angles and stack in the helix, with A22 slightly above A34 in a staggered arrangement (Figure 4A). This stacking of A22 and A34 in the helix does not significantly disrupt the A-form helical character of the surrounding base pairs in the stem. However, the C1′–C1′ cross-strand distance, indicative of minor groove width, between A22 and A34 is slightly decreased from the normal A-form distance of 11 Å down to 10 Å.

The helix II stem is capped by a well-defined, structured pentaloop (Figure 4B). The first two nucleotides, G26 and U27, stack on the 5′ side of the loop with G26 stacking directly over the U25·A31 closing base pair. The U27 base is rotated into the major groove, with its H5–H6 face orientated closer to its sugar moiety and its Watson–Crick face pointing into the major groove. The twisting of U27 can be attributed to its C2′-*endo* sugar conformation and a *trans* ε angle causing rotation around the glycosidic bond. The turn in the phosphodiester backbone occurs between U27 and A28, evidenced by the opposite orientation of the sugar moieties. A28 is located at the top of the loop, lying along the minor groove with its Watson–Crick face pointing downward toward the helical axis (Figure 4B). A29 adopts a *syn* conformation with its base located over its sugar and the base is in the major groove with its Watson–Crick face exposed to solvent. The A29 H8 proton is situated in the center of the pentaloop, with NOEs to the U27 H5 and H6 protons as well as the A28 H8 and sugar resonances. U30 NOEs are consistent with weak stacking on A31, and the NOEs from the U30 H5 and H6 protons across the stem to the U27 H1′ as well as to the A29 H2′ and H3′ are consistent with the location

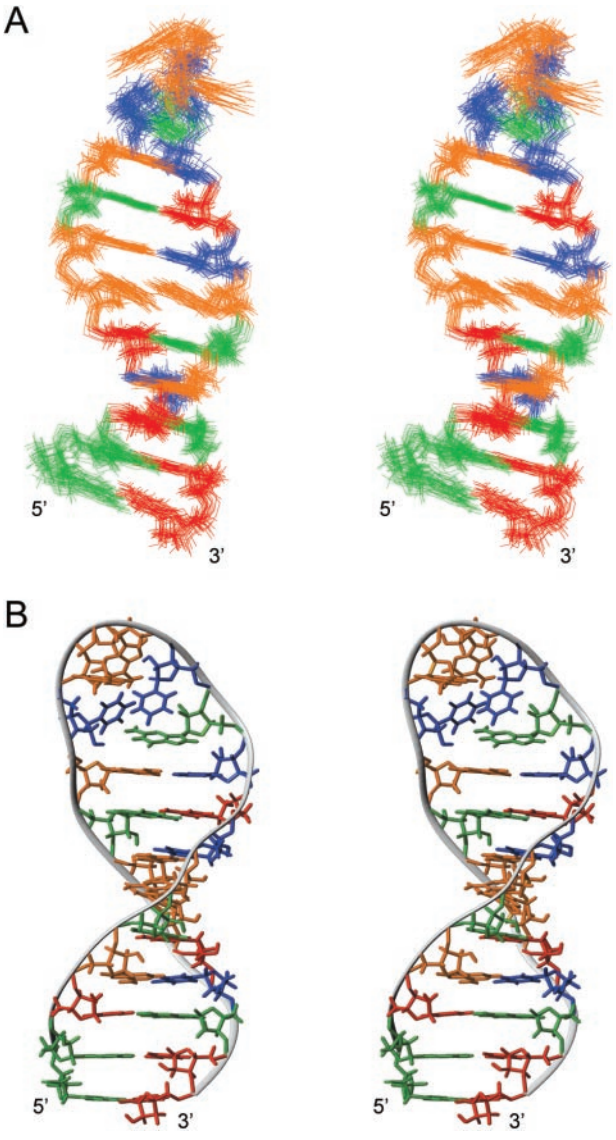

Figure 3. Solution structure of TBE_{HP}. (**A**) Stereoview of the 20 lowest energy structures. Nucleotides are colored A (orange), U (blue), C (red) and G (green). (**B**) Stereoview of the lowest energy structure of TBE_{HP} rotated 60° clockwise with respect to (A) for a better view of the loop structure. The gray ribbon through the phosphate atoms is used to indicate the backbone topology.

of the base in the minor groove of the loop. As is the case with U27, the C2′-*endo* sugar conformation and *trans* ε angle of U30 cause a twisting of the base around the glycosidic bond back into the minor groove with the plane of the base at an 80° angle compared with the plane of the closing U25·A31 base pair (Figure 4B).

DISCUSSION

Tetrahymena helix II is structured in the absence of TERT

Helix II of the *T.thermophila* telomerase RNA was previously proposed to be unstructured in the absence of TERT, based on enzymatic footprinting of TER with RNase T1 and RNase V1 in the absence and presence of TERT in rabbit reticulocyte lysate (RRL) (40). Cleavage of the free TER with RNase T1, which cleaves 3′ of single-stranded guanine nucleotides, indicated moderate cleavage 3′ of all of the guanine nucleotides (G21, G26, G32 and G37) present in helix II. A change in the RNase T1 cleavage pattern was observed upon the addition of TERT. In the presence of TERT, no cleavage was observed for G21, G32 and G37 while moderate cleavage was still observed for G26, which is located in the pentaloop of helix II. Cleavage of free TER with RNase V1, which cleaves base paired nucleotides, showed strong cleavage toward the terminal end of the helix, the A20·U36 and G21·C35 base pairs, but very weak cleavage for the three Watson–Crick base pairs in the upper stem, U23·A33, C24·G32 and U25·A31. In the presence of TERT, the RNase V1 cleavage pattern of the TER does not change for the terminal end of the helix, but the cleavage of the base pairs at the upper stem of helix II is increased. These results led to the hypothesis that TER undergoes a conformational change upon the binding of TERT. An element of this postulated conformational change is the conversion of helix II from an unstructured region in the absence of TERT to a structured helix in the presence of TERT. Our results show that helix II of TBE_{WT} is, in fact, structured in the absence of TERT. However, the relatively low stability (T_m = 46.4°C) of TBE_{WT} would make this helix susceptible to RNase cleavage. NMR spectra of exchangeable resonances of both TBE_{WT} and TBE_{HP} (Figure 2A and data not shown) show much less intense peaks and cross peaks for the U23·A33 and U25·A31 base pairs than for other Watson–Crick base pairs in the helical stem, consistent with the decreased RNase V1 cleavage in the upper portion of the stem compared with the terminal region. All of the guanine nucleotides in helix II were moderately cleaved by RNase T1 in the absence of TERT. G26 is single-stranded (in the pentaloop) and should be cleaved in both the free and bound TER unless it is a direct site for TERT binding. G32 is located between the two A·U base pairs in the upper stem which both exhibit only modest RNase V1 cleavage suggesting weak hydrogen bonding. G21 is the nucleotide directly 5′ to the staggered adenine nucleotides in the helical stem, and modest changes in the A-form helical structure in this region may expose the 3′ side of G21 to increased RNase T1 cleavage. G37 is in the terminal base pair of the TBE helix, and modest RNase T1 cleavage is consistent with fraying of the base pairs at the helix terminus. Therefore, the positions of the guanine nucleotides in the TBE make them likely candidates for RNase T1 cleavage, even though the region is structured. Thus, while structure probing results suggest that binding of TERT to TER may increase the stability of the helix or decrease accessibility, TERT binding is not a prerequisite for helix II structure formation.

Conservation of the helix II sequence

Twelve holotrichous *Tetrahymena* telomerase sequences are available in the telomerase literature (41–43) and the Rfam database (http://www.sanger.ac.uk/Software/Rfam) (44). The sequence of helix II, from C15 to A40 (Figure 1A), is at least 70% conserved at each nucleotide position with the exception of two nucleotides, G26 and A34, omitting *T.paravorax*, which lacks this helix completely. The stem of helix II in most *Tetrahymena* species has roughly the same thermodynamic stability, and in all cases, the region of the stem

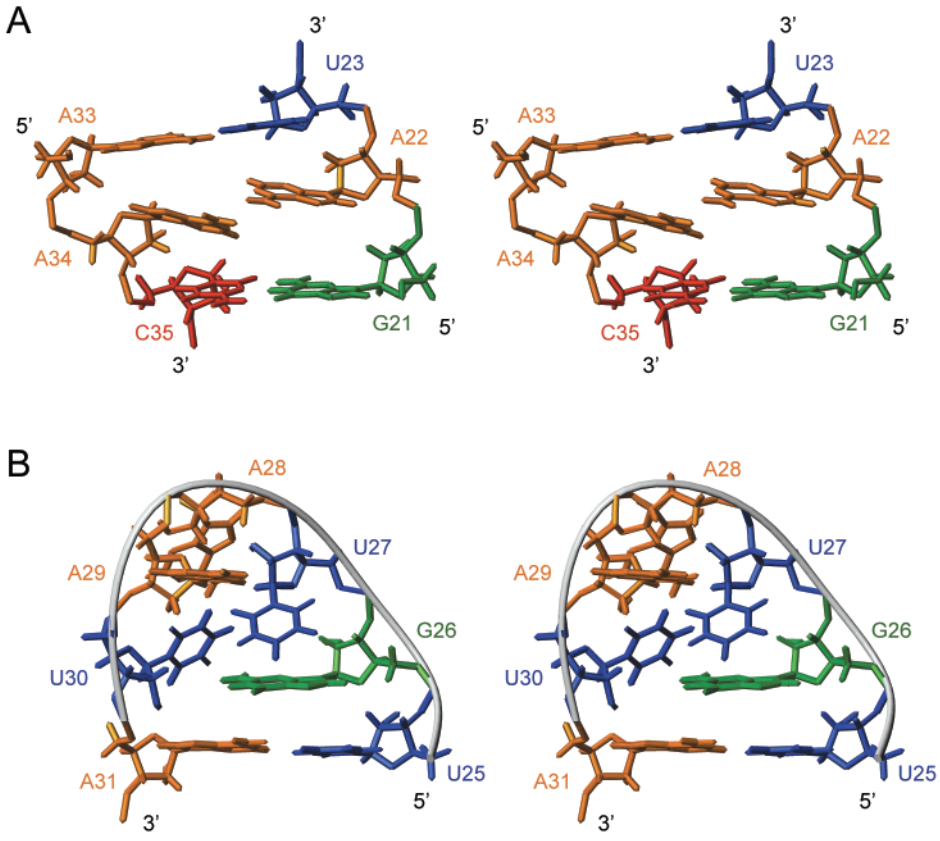

Figure 4. Features of the TBE_{HP} structure. (**A**) Stereoview of the lowest energy structure showing the staggered arrangement of A22 and A34 in the middle of the helical stem. (**B**) Stereoview of the major groove view of the lowest energy structure of the TBE_{HP} pentaloop. Nucleotides are colored as described in Figure 3.

where the adenine–adenine internal loop (or mismatch) is located in *T.thermophila* possesses the weakest stacking interaction in the entire stem, even when these nucleotides are not both adenines. The sequence conservation of the helix II terminal base pair C19·G37 may be required for stabilization of this helical stem. The sequence of the pentaloop which caps helix II is conserved among the species in the holotrichous *Tetrahymena* genus to be a DUWAU motif, where D = G, A or U and W = A or U (42,43). The second (U), fourth (A) and final (U) positions in the pentaloop are absolutely conserved. Although *T.paravorax* is classified as a holotrichous ciliate, phylogenies based on ribosomal RNA sequences and the histone H3II/H4II intergenic region indicate that it is just as closely related to hypotrichous ciliates as it is to the closest *Tetrahymena* species (45,46). The telomerase RNA secondary structures from the hypotrichous ciliates, such as *Oxytricha nova*, lack helix II completely, suggesting the *T.paravorax* TER secondary structure may be more closely related to this suborder (42).

The first nucleotide in the TBE loop is the least conserved. Any single-stranded nucleotide immediately following an A-form stem can stack on the stem and increase thermodynamic stability, although there are different energetic contributions based on base-pair and single-stranded nucleotide sequence (47). Consistent with this, G26 contributes to the overall stability by stacking over the terminal base pair, but there is no evidence for any hydrogen bonding or sequence specific interactions between G26 and other nucleotides in the loop (Figure 4B). Interestingly, the 3 nt that are conserved in the *Tetrahymena* species (U27, A29 and U30) all display unusual structural properties in the pentaloop. Both U27 and U30 have ε dihedral angles in the *trans* range, instead of the *gauche*$^-$ orientation more commonly found in RNA, and A29 is in the *syn* conformation (Figure 4B). *Syn* adenine nucleotides are rare in RNA tertiary structure; we found only one other RNA structure, the crystal structure of a synthetic RNA octamer with adenine overhangs, that has *syn* adenosines (48). The middle loop nucleotide, A28, is conserved to be either an A or U. The structural basis for this conservation is not evident from the structure, as the nucleotide in this position lies along the minor groove face of the loop with its Watson–Crick face exposed to solvent. The *Tetrahymena* helix II loop sequence could be partially conserved in order to either make sequence specific contacts or generate a loop structural orientation for interaction with the rest of the telomerase RNA or the protein components of the holoenzyme.

Comparison to 16S rRNA pentaloop

The structural characterization of the small ribosomal subunit from *Thermus thermophilus* (49) and large ribosomal subunit from *Haloarcula marismortui* (23) has revealed a large number of structured RNA pentaloops involved in tertiary interactions with both proteins and RNA. These pentaloops play roles in RNA–protein interactions and long-range RNA–RNA interactions essential in establishing the overall tertiary structure of the ribosome. In addition to ribosomal RNA,

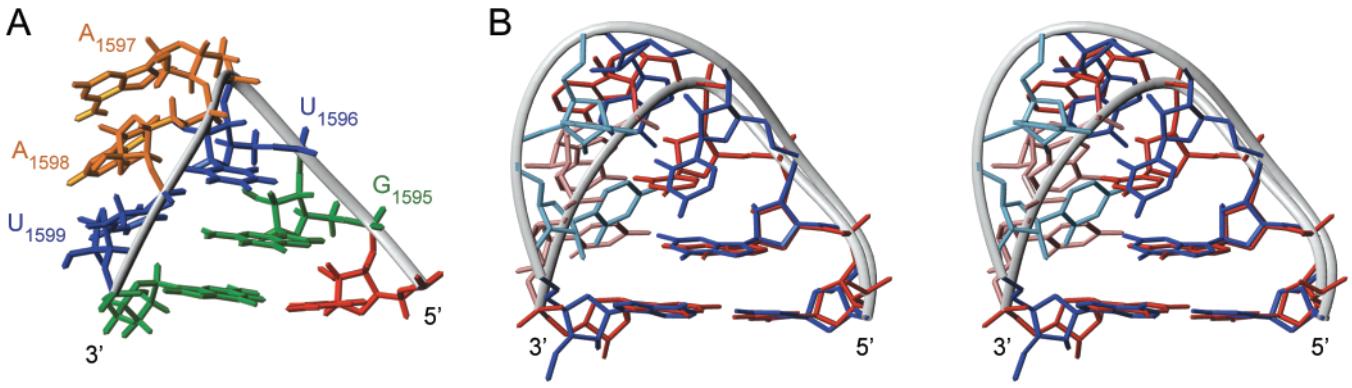

Figure 5. The GUAAU pentaloop. (**A**) The X-ray crystal structure of a GUAAU pentaloop from the *H.marismortui* 23S large ribosomal subunit (PDB code 1FFX) (23) colored by nucleotide as described in Figure 3. (**B**) Overlay of the TER (blue) and rRNA (red) GUAAU pentaloops. The nucleotides which differ most in position from each other are highlighted by a lighter shade of blue or red in the TER and rRNA loops, respectively.

structured pentaloops have been identified in other biological systems including pre-mRNA splicing machinery, tRNAs, ADARs (adenosine deaminases that act on RNA) and human telomerase (50–55).

The primary sequence of the pentaloop presented here from the *T.thermophila* telomerase RNA, 5′-$G_1U_2A_3A_4U_5$-3′, is also found in a pentaloop (nt 1595–1599) in the 23S rRNA of the 50S large ribosomal subunit of *H.marismortui* (Figure 5A) (23). Comparison of the two pentaloops (Figures 4B and 5A) reveals that the first 3 nt, 5′-$G_1U_2A_3$, are nearly identical in both pentaloop structures with G_1 in the 5′ stack, U_2 stacking on G_1 with near A-form geometry but with its H5–H6 face twisted toward the sugar moiety, the turn of the phosphodiester backbone between U_2 and A_3, and A_3 lying at the top of the loop in the minor groove. However, the structures are very different for the last two nucleotides in the pentaloop, A_4U_5-3′ (Figure 5B). The A_4 nucleotide in the TER is in the *syn* conformation and the base is on the major groove face of the loop. The same adenosine in the 23S rRNA is in the *anti* conformation which allows stacking of the $A_3A_4U_5$-3′ sequence along the minor groove face of the loop.

The differences between the rRNA and TER 5′-GUAAU-3′ pentaloop structures may be due to the different conditions under which each structure was investigated. The rRNA pentaloop was solved in the context of the 50S large ribosomal subunit and interacts with both a ribosomal protein and RNA, while the TER pentaloop was solved in the absence of other RNA and protein cofactors and thus demonstrates the free conformation of the pentaloop. It is not surprising that the rRNA and TER pentaloops adopt slightly different structures as RNA and protein conformational changes upon binding have previously been observed (56–58). The rRNA 5′-GUAAU-3′ pentaloop makes both RNA and protein contacts, interacting with ribosomal protein L19e on its major groove face and a long-range RNA–RNA contact on the minor groove face of the pentaloop. A stretch of positively charged amino acid residues interact with the negatively charged phosphodiester backbone along the major groove of the pentaloop involving G_{1595}, U_{1596} and A_{1597} (Figure 5A). The second adenine in the pentaloop, A_{1598}, is inserted into the minor groove of a neighboring RNA helix in an A-minor motif (59).

The interactions of the rRNA 5′-GUAAU-3′ pentaloop with both protein and RNA suggest possible interactions for the TER 5-GUAAU-3′ pentaloop with the telomerase RNA itself or one of the holoenzyme protein components of telomerase. The *T.thermophila* telomerase holoenzyme contains five proteins components, TERT, p20, p45, p65 and p75 (8). Helix II's pentaloop may be involved in recruitment or binding interactions with one of these proteins or may aid in the overall stabilization of the telomerase RNP complex. A conformational change within TER has previously been predicted upon protein binding (40) which may place other regions of the TER RNA in proximity to the helix II terminal pentaloop. The structural analysis presented here lays the foundation for future biochemical and structural studies to determine the role and possible interactions for the helix II pentaloop in the *Tetrahymena* telomerase holoenzyme.

Implications of the helix II structure for template boundary definition in *Tetrahymena* telomerase

Proper definition of the template boundary is essential to ensure high fidelity addition of the precise telomeric repeat sequence to the ends of the telomeres (19,20,22,60). Systematic mutational analysis followed by conventional telomerase assays that measure the products of telomerase elongation directly has lead to the identification of the elements responsible for 5′ template boundary definition in ciliates, yeast, and mammalian telomerase RNA (20,22,60).

In all species where a TBE has been identified, the telomerase RNA structure plays an essential role in template boundary definition (20,22,60). Although the specific structures of the TBE elements from ciliates, yeast, and mammals appear quite divergent, they do share some similarities. Template boundary elements are all located close to, and 5′ of, the template sequence. In yeast, a helix directly 5′ of the template sequence acts as the template boundary element, and mutations that affect base pairing ability lead to improper template 5′ boundary definition (60). In mammals, the helix P1b is responsible for template boundary definition (22) and is located 6–11 nt 5′ of the template sequence (61). Disruption of the P1b helix base pairing or alteration of the distance between helix P1b and the template sequence leads to improper incorporation of telomeric repeats onto telomeres (22).

In ciliates, the TBE is defined by specific nucleotides in the single-stranded regions 5′ and 3′ of helix II as well as the requirement for base pairing at the end of helix II (the C19·G37 base pair, Figure 1A), implying both sequence and structural requirements (20). Mutations affecting the base pairing at the end of helix II, as well as the conserved single-stranded nucleotides 5′ and 3′ of helix II, resulted in copying telomeric repeats beyond the normal length (20). Although the TBE has been identified in telomerase RNAs from a wide variety of species, the mechanism(s) through which template boundary definition is accomplished remains unknown as well as whether there is a single universal mechanism among species.

A model for the mechanism of template boundary definition in vertebrate telomerase has been proposed by Chen and Greider (22). In this model, the TBE constrains the RNA template within the catalytic active site of TERT through either RNA base pairing present in the telomerase RNA or through RNA–protein interactions induced upon TERT binding. The TBE of *Tetrahymena* telomerase, which includes the terminal end of helix II and its 5′ and 3′ single-stranded nucleotides, appears to employ base pairing which is essential for proper 5′ definition of the template as well as high affinity TERT binding (20,21). Although it was previously proposed that helix II from the TER did not adopt a helical structure in the absence of TERT binding (40), the TBE does form an ordered, helical structure even when TERT is not bound. This suggests that a structured TBE element may act as a scaffold for TERT or other holoenzyme protein binding and may be crucial in the correct positioning the template sequence and the TERT active site for proper addition of telomeric repeats, consistent with the proposed model for vertebrate telomerase.

ACKNOWLEDGEMENTS

This work was supported by NSF grant MCB 051770 and NIH grant GM048123 to J.F. The authors thank Robert Peterson for technical NMR assistance and Evan Feinstein for help with manuscript and figure preparation. Funding to pay the Open Access publication charges for this article was provided by NSF grant MCB 081770.

Conflict of interest statement. None declared.

REFERENCES

1. Shore,D. (1997) Telomerase and telomere-binding proteins: controlling the endgame. *Trends Biochem. Sci*., **22**, 233–235.
2. Greider,C.W. (1996) Telomere length regulation. *Annu. Rev. Biochem*., **65**, 337–365.
3. McEachern,M.J. and Blackburn,E.H. (1995) Runaway telomere elongation caused by telomerase RNA gene mutations. *Nature*, **376**, 403–409.
4. Kirk,K.E., Harmon,B.P., Reichardt,I.K., Sedat,J.W. and Blackburn,E.H. (1997) Block in anaphase chromosome separation caused by a telomerase template mutation. *Science*, **275**, 1478–1481.
5. Guiducci,C., Cerone,M.A. and Bacchetti,S. (2001) Expression of mutant telomerase in immortal telomerase-negative human cells results in cell cycle deregulation, nuclear and chromosomal abnormalities and rapid loss of viability. *Oncogene*, **20**, 714–725.
6. Greider,C.W. and Blackburn,E.H. (1985) Identification of a specific telomere terminal transferase activity in *Tetrahymena* extracts. *Cell*, **43**, 405–413.
7. Collins,K. (1999) Ciliate telomerase biochemistry. *Annu. Rev. Biochem*., **68**, 187–218.
8. Witkin,K.L. and Collins,K. (2004) Holoenzyme proteins required for the physiological assembly and activity of telomerase. *Genes Dev*., **18**, 1107–1118.
9. Cech,T.R., Nakamura,T.M. and Lingner,J. (1997) Telomerase is a true reverse transcriptase. *Biochemistry (Mosc.)*, **62**, 1202–1205.
10. Chen,J.L. and Greider,C.W. (2004) Telomerase RNA structure and function: implications for dyskeratosis congenital. *Trends Biochem. Sci*., **29**, 183–192.
11. Chen,J.L. and Greider,C.W. (2004) An emerging consensus for telomerase RNA structure. *Proc. Natl Acad. Sci. USA*, **101**, 14683–14684.
12. Lin,J., Ly,H., Hussain,A., Abraham,M., Pearl,S., Tzfati,Y., Parslow,T.G. and Blackburn,E.H. (2004) A universal telomerase RNA core structure includes structured motifs required for binding the telomerase reverse transcriptase protein. *Proc. Natl Acad. Sci. USA*, **101**, 14713–14718.
13. O'Connor,C.M., Lai,C.K. and Collins,K. (2005) Two purified domains of telomerase reverse transcriptase reconstitute sequence-specific interactions with RNA. *J. Biol. Chem*., **280**, 17533–17539.
14. Miller,M.C. and Collins,K. (2002) Telomerase recognizes its template by using an adjacent RNA motif. *Proc. Natl Acad. Sci. USA*, **99**, 6585–6590.
15. Gilley,D. and Blackburn,E.H. (1999) The telomerase RNA pseudoknot is critical for the stable assembly of a catalytically active ribonucleoprotein. *Proc. Natl Acad. Sci. USA*, **96**, 6621–6625.
16. Lai,C.K., Miller,M.C. and Collins,K. (2003) Roles for RNA in telomerase nucleotide and repeat addition processivity. *Mol. Cell*, **11**, 1673–1683.
17. Mason,D.X., Goneska,E. and Greider,C.W. (2003) Stem-loop IV of *Tetrahymena* telomerase RNA stimulates processivity in *trans*. *Mol. Cell. Biol*., **23**, 5606–5613.
18. Prathapam,R., Witkin,K.L., O'Connor,C.M. and Collins,K. (2005) A telomerase holoenzyme protein enhances telomerase RNA assembly with telomerase reverse transcriptase. *Nature Struct. Mol. Biol*., **12**, 252–257.
19. Autexier,C. and Greider,C.W. (1995) Boundary elements of the *Tetrahymena* telomerase RNA template and alignment domains. *Genes Dev*., **9**, 2227–2239.
20. Lai,C.K., Miller,M.C. and Collins,K. (2002) Template boundary definition in *Tetrahymena* telomerase. *Genes Dev*., **16**, 415–420.
21. Licht,J.D. and Collins,K. (1999) Telomerase RNA function in recombinant *Tetrahymena* telomerase. *Genes Dev*., **13**, 1116–1125.
22. Chen,J.L. and Greider,C.W. (2003) Template boundary definition in mammalian telomerase. *Genes Dev*., **17**, 2747–2752.
23. Ban,N., Nissen,P., Hansen,J., Moore,P.B. and Steitz,T.A. (2000) The complete atomic structure of the large ribosomal subunit at 2.4 Å resolution. *Science*, **289**, 905–920.
24. Klein,D.J., Moore,P.B. and Steitz,T.A. (2004) The roles of ribosomal proteins in the structure assembly, and evolution of the large ribosomal subunit. *J. Mol. Biol*., **340**, 141–1477.
25. Dieckmann,T. and Feigon,J. (1997) Assignment methodology for larger oligonucleotides: application to an ATP-binding RNA aptamer. *J. Biomol. NMR*, **9**, 259–272.
26. Theimer,C.A., Wang,Y., Hoffman,D.W., Krisch,H.M. and Giedroc,D.P. (1998) Non-nearest neighbor effects on the thermodynamics of unfolding of a model mRNA pseudoknot. *J. Mol. Biol*., **279**, 545–564.
27. Cromsigt,J., van Buuren,B., Schleucher,J. and Wijmenga,S.S. (2001) In James,T., Dotsch,V. and Schmitz,U. (eds), *Methods in Enzymology*. Academic Press, San DiegoVol. 338, pp. 371–399.
28. Luy,B. and Marino,J.P. (2000) Direct evidence for Watson–Crick base pairs in a dynamic region of RNA structure. *J. Am. Chem. Soc*., **122**, 8095–8096.
29. Majumdar,A., Kettani,A., Skripkin,E. and Patel,D.J. (2001) Pulse sequences for detection of NH2·N hydrogen bonds in sheared G·A mismatches via remote, non-exchangeable protons. *J. Biomol. NMR*, **19**, 103–113.
30. Simorre,J.P., Zimmermann,G.R., Mueller,L. and Pardi,A. (1996) Triple-resonance experiments for assignment of adenine base resonances in C^{13}/N^{15}-labeled RNA. *J. Am. Chem. Soc*., **118**, 5316–5317.
31. Legault,P., Jucker,F.M. and Pardi,A. (1995) Improved measurement of ^{13}C, ^{31}P J coupling constants in isotopically labeled RNA. *FEBS Lett*., **362**, 156–160.

32. Kolk,M.H., Wijmenga,S.S., Heus,H.A. and Hilbers,C.W. (1998) On the NMR structure determination of a 44n RNA pseudoknot: Assignment strategies and derivation of torsion angle restraints. *J. Biomol. NMR*, **12**, 423–433.
33. Sklenar,V., Miyashiro,H., Zon,G., Miles,H.T. and Bax,A. (1986) Assignment of the ^{31}P resonances in oligonucleotides by two-dimensional NMR spectroscopy. *FEBS Lett*., **208**, 94–98.
34. de Alba,E. and Tjandra,N. (2002) NMR dipolar couplings for the structure determination of biopolymers in solution. *Prog. Nucl. Magn. Reson. Spectros*., **40**, 175–197.
35. Wu,H., Pok,K., Butcher,S.E., Kang,S., Chanfreau,G. and Feigon,J. (2001) A novel family of RNA tetraloop structure forms the recognition site for *S.cerevisiae* RNase III. *EMBO J*., **20**, 7240–7249.
36. Wijmenga,S.S. and van Buuren,B.N.M. (1998) The use of NMR methods for conformational studies of nucleic acids. *Prog. Nucl. Magn. Reson. Spectros*., **32**, 287–387.
37. Brunger,A.T. (1992) *X-PLOR, version 3.1. A system for X-ray crystallography and NMR*. Yale University Press, New Haven, CT.
38. Schwieters,C.D., Kuszewski,J.J., Tjandra,N. and Clore,G.M. (2003) The X-PLOR-NIH NMR molecular structure determination package. *J. Magn. Reson*., **160**, 65–73.
39. Koradi,R., Billeter,M. and Wüthrich,K. (1996) MOLMOL—a program for display and analysis of macromolecular structures. *J. Mol. Graphics*, **14**, 51–55.
40. Sperger,J.M. and Cech,T.R. (2001) A stem–loop of *Tetrahymena* telomerase RNA distant from the template potentiates RNA folding and telomerase activity. *Biochemistry*, **40**, 7005–7016.
41. Lingner,J., Hendrick,L.L. and Cech,T.R. (1994) Telomerase RNAs of different ciliates have a common secondary structure and a permuted template. *Genes Dev*., **8**, 1984–1998.
42. McCormick-Graham,M. and Romero,D.P. (1995) Ciliated telomerase RNA structural features. *Nucleic Acids Res*., **23**, 1091–1097.
43. Ye,A.J. and Romero,D.P. (2002) Phylogenetic relationships amongst *tetrahymenine* ciliates inferred by a comparison of telomerase RNAs. *Intl. J. Syst. Evol. Microbiol*., **52**, 2297–2302.
44. Griffiths-Jones,S., Bateman,A., Marshall,M., Khanna,A. and Eddy,S.R. (2003) Rfam: an RNA family database. *Nucleic Acids Res*., **33**, 439–441.
45. Preparata,R.M., Meyer,E.B., Preparata,F.P., Simon,E.M., Vossbrinck,C.R. and Nanney,D.L. (1989) Ciliate evolution: the ribosomal phylogenies of the *tetrahymenine* ciliates. *J. Mol. Evol*., **28**, 427–441.
46. Brunk,C.F., Kahn,R.W. and Sadler,L.A. (1990) Phylogenetic relationships among *Tetrahymena* species determined using the polymerase chain reaction. *J. Mol. Evol*., **30**, 290–297.
47. Turner,D.H., Sugimoto,N. and Freier,S.M. (1988) RNA structure prediction. *Ann. Rev. Biophys. Biophys. Chem*., **17**, 167–192.
48. Shi,K., Biswas,R., Mitra,S.N. and Sundaralingam,M. (2000) The crystal structure of the octamer [r(guauaca)dC]2 with six Watson–Crick base-pairs and two 3′ overhang residues. *J. Mol. Biol*., **299**, 113–122.
49. Wimberly,B.T., Brodersen,D.E., Clemons,W.M.,Jr, Morgan-Warren,R.J., Carter,A.P., Vonrhein,C., Hartsch,T. and Ramakrishnan,V. (2000) Structure of the 30S ribosomal subunit. *Nature*, **407**, 327–339.
50. Sashital,D.G., Allmann,A.M., Van Doren,S.R. and Butcher,S.E. (2003) Structural basis for a lethal mutation in U6 RNA. *Biochemistry*, **42**, 1470–1477.
51. Huppler,A., Nikstad,L.J., Allmann,A.M., Brow,D.A. and Butcher,S.E. (2002) Metal binding and base ionization in the U6 RNA intramolecular stem–loop structure. *Nature Struct. Biol*., **9**, 431–435.
52. Cabello-Villegas,J., Winkler,M.E. and Nikonowicz,E.P. (2002) Solution conformations of unmodified and $A_{37}N^6$-dimethylallyl modified anticodon stem–loops of *Escherichia coli* tRNA(Phe). *J. Mol. Biol*., **319**, 1015–1034.
53. Yaremchuk,A., Tukalo,M., Grotli,M. and Cusack,S. (2001) A succession of substrate induced conformational changes ensures the amino acid specificity of *Thermus thermophilus* prolyl-tRNA synthetase: comparison with histidyl-tRNA synthetase. *J. Mol. Biol*., **309**, 989–1002.
54. Stefl,R. and Allain,F.H. (2005) A novel RNA pentaloop fold involved in targeting ADAR2. *RNA*, **11**, 592–597.
55. Theimer,C.A., Finger,L.D. and Feigon,J. (2003) YNMG tetraloop formation by a dyskeratosis congenita mutation in human telomerase RNA. *RNA*, **9**, 1446–1455.
56. Williamson,J.R. (2000) Induced fit in RNA–protein recognition. *Nature Struct. Biol*., **7**, 834–837.
57. Allain,F.H.-T., Bouvet,P., Dieckmann,T. and Feigon,J. (2000) Molecular basis of sequence specific recognition of RNA stem–loops by nucleolin. *EMBO J*., **19**, 6870–6881.
58. Leulliot,N. and Varani,G. (2001) Current topics in RNA–protein recognition: Control of specificity and biological function through induced fit and conformational capture. *Biochemistry*, **40**, 7947–7956.
59. Nissen,P., Ippolito,J.A., Ban,N., Moore,P.B. and Steitz,T.A. (2001) RNA tertiary interactions in the large ribosomal subunit: the A-minor motif. *Proc. Natl Acad. Sci. USA*, **98**, 4899–4903.
60. Tzfati,Y., Fulton,T.B., Roy,J. and Blackburn,E.H. (2000) Template boundary in a yeast telomerase specified by RNA structure. *Science*, **288**, 863–867.
61. Chen,J.L., Blasco,M.A. and Greider,C.W. (2000) Secondary structure of vertebrate telomerase RNA. *Cell*, **100**, 503–514.